Behaviour of Granular Soils Under Uni- and Multidimensional Drained High-Cyclic Loading

Torsten Wichtmann[1(✉)] and Lukas Knittel[2]

[1] Chair for Soil Mechanics, Foundation Engineering and Environmental Geotechnics, Ruhr-University Bochum, Universitätsstraße 150, 44789 Bochum, Germany
torsten.wichtmann@rub.de

[2] Karlsruhe Institute of Technology, Institute of Soil Mechanics and Rock Mechanics, Engler-Bunte-Ring 14, 76131 Karlsruhe, Germany
lukas.knittel@kit.edu

Abstract. The paper summarizes a long-term experimental research program on the behaviour of granular soils under high-cyclic loading, that means a loading with many cycles ($N \geq 10^3$) and relatively small strain amplitudes ($\varepsilon^{\mathrm{ampl}} \leq 10^{-3}$). Numerous drained cyclic triaxial and hollow cylinder triaxial tests have been performed, most of them on Karlsruhe fine sand. The effects of the stress or strain amplitude, average stress, relative density, grain size distribution curve, particle shape and a content of non-plastic fines or shell fragments on the cumulative deformations are discussed. The important role of initial fabric (sample preparation method) is demonstrated, while the geometry and dimensions of the samples seem to be of secondary importance. The effect of multiple changes of the polarization (i.e. direction) of the cycles was found less important than previously thought. The bundling of a cyclic loading with continuously changing amplitude into bundles of cycles each with a constant amplitude is demonstrated to be conservative. An interesting effect has been observed in tests with bundles of cycles interrupted by monotonic loading phases: The monotonic loading can lead to a loss of the cyclic preloading memory, and thus to an increase of the rate of strain accumulation in the next bundle of cycles. Results from tests with 1D, 2D, 3D and 4D stress and strain paths confirm the amplitude definition for multi-dimensional strain loops incorporated into a high-cycle accumulation (HCA) model. The description of the strain accumulation rates by the HCA model is discussed based on the results from the various test series.

1 Introduction

A high-cyclic loading may be caused by traffic (e.g. high-speed trains, magnetic levitation trains), industrial sources (e.g. crane rails, machine foundations), wind and waves (e.g. on-shore and off-shore wind turbines, coastal structures),

T. Triantafyllidis (Ed.): *Recent Developments of Soil Mechanics and Geotechnics in Theory and Practice*, LNACM 91, pp. 136–165, 2020.
https://doi.org/10.1007/978-3-030-28516-6_8

repeated filling and emptying processes (e.g. locks, tanks and silos), construction processes (e.g. vibration of sheet piles) or mechanical compaction (e.g. vibratory compaction). Permanent deformations caused by such high-cyclic loading may endanger the serviceability of foundations and thus must be accurately predicted in the design stage. For that purpose a high-cycle accumulation (HCA) model has been developed by Niemunis et al. [10]. It is based on an extensive laboratory study with drained cyclic tests on various sands [18]. The most important findings of that and subsequent experimental work [19] are summarized herein. The consideration of the various parameters in the HCA model is discussed.

If not otherwise stated in the following sections, the tests were performed in a cyclic triaxial device using samples of 10 cm diameter and 10 cm height. A scheme of the devices at IBF, KIT is shown in Fig. 1. The samples were prepared by air pluviation and tested in the water-saturated condition using a back pressure of 200 or 500 kPa. The effective lateral stress σ_3' was kept constant, while the cyclic loading was applied in the vertical direction, with an average value of effective axial stress $\sigma_1'^{\mathrm{av}}$ and a stress amplitude $\sigma_1'^{\mathrm{ampl}}$. The cyclic loading was realized by means of a pneumatic loading system. In this paper the stress conditions in a test are described by the average mean pressure p^{av} (with $p = (\sigma_1' + 2\sigma_3')/3$), the average deviatoric stress q^{av} (with $q = \sigma_1' - \sigma_3'$), average stress ratio $\eta^{\mathrm{av}} = q^{\mathrm{av}}/p^{\mathrm{av}}$ and deviatoric stress amplitude $q^{\mathrm{ampl}} = \sigma_1'^{\mathrm{ampl}}$.

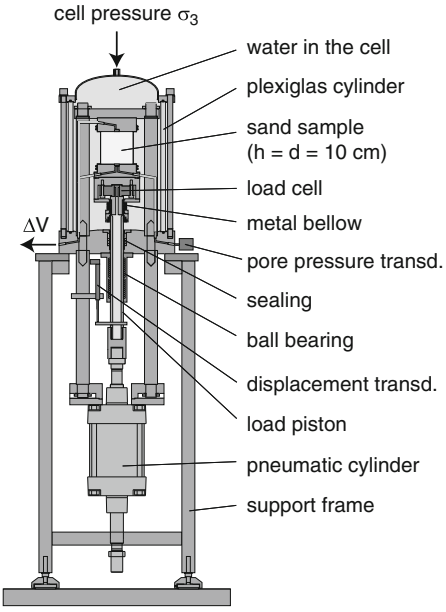

Fig. 1. Scheme of the cyclic triaxial devices at IBF, KIT

Axial deformations were measured with a displacement transducer attached to the load piston, while volume changes were obtained from a burette system

connected to the fully water-saturated pore space, using a differential pressure transducer. The axial strain ε_1 and the volumetric strain $\varepsilon_v = \varepsilon_1 + 2\varepsilon_3$ derived from these measurements are used to calculate the lateral strain $\varepsilon_3 = (\varepsilon_v - \varepsilon_1)/2$ and the deviatoric strain $\varepsilon_q = 2/3(\varepsilon_1 - \varepsilon_3)$. The total strain is defined as $\varepsilon = \|\boldsymbol{\varepsilon}\| = \sqrt{(\varepsilon_1)^2 + 2(\varepsilon_3)^2}$, i.e. as the norm of the strain tensor. All these strain quantities can be splitted into a resilient/elastic/amplitude portion $\sqcup^{\mathrm{ampl}}$ and a residual/plastic/accumulated portion $\sqcup^{\mathrm{acc}}$. In the context of a HCA model a rate is understood as the derivative of a variable with respect to the number of cycles, e.g. $\dot{\sqcup} = \partial \sqcup / \partial N$.

The first *irregular* cycle usually generates larger deformations and is thus applied with a relative low frequency (0.01 Hz). The subsequent 10^5 regular cycles are applied with a higher frequency of 0.2 Hz. Since the HCA model predicts the strain accumulation rates during the regular cycles only, the first irregular cycle is not discussed in this paper. In the following, $N = 1$ thus refers to the end of the first regular cycle.

In the HCA model the tensor of the rate of strain accumulation is described by $\dot{\boldsymbol{\varepsilon}}^{\mathrm{acc}} = \dot{\varepsilon}^{\mathrm{acc}}\mathbf{m}$, i.e. as the product of the scalar *intensity* of strain accumulation $\dot{\varepsilon}^{\mathrm{acc}} = \|\dot{\boldsymbol{\varepsilon}}^{\mathrm{acc}}\|$ (norm of strain rate tensor) and the *direction* of accumulation $\mathbf{m} = \dot{\boldsymbol{\varepsilon}}^{\mathrm{acc}}/\|\dot{\boldsymbol{\varepsilon}}^{\mathrm{acc}}\|$ (unit tensor). In the triaxial case, the intensity of accumulation is calculated as $\dot{\varepsilon}^{\mathrm{acc}} = \partial\varepsilon^{\mathrm{acc}}/\partial N$ and the direction of accumulation can be expressed by the ratio of the volumetric and deviatoric strain accumulation rates $\dot{\varepsilon}_v^{\mathrm{acc}}/\dot{\varepsilon}_q^{\mathrm{acc}}$. In the following the test results are analyzed with respect to both, the measured intensity of accumulation $\dot{\varepsilon}^{\mathrm{acc}}$ or their integral value $\varepsilon^{\mathrm{acc}}$, and the direction of accumulation $\dot{\varepsilon}_v^{\mathrm{acc}}/\dot{\varepsilon}_q^{\mathrm{acc}}$.

Most of the test series presented herein have been performed at the Institute of Soil Mechanics and Rock Mechanics (IBF) at Karlsruhe Institute of Technology (KIT). The only exception is the study on the influence of the grain size distribution curve documented in Sect. 3. Those tests have been conducted at the Chair for Foundation Engineering and Soil Mechanics at Ruhr-University Bochum (RUB).

2 Stress or Strain Amplitude, Soil Density and Average Stress

The influence of the soil density and the average and cyclic stresses is inspected based on a series with 17 drained cyclic triaxial tests performed on Karlsruhe fine sand (KFS), a clean fine sand with mean grain size $d_{50} = 0.14$ mm and uniformity coefficient $C_u = d_{60}/d_{10} = 1.5$. Four different stress amplitudes ($20\,\mathrm{kPa} \leq q^{\mathrm{ampl}} \leq 80\,\mathrm{kPa}$), seven different initial relative densities ($0.25 \leq I_{D0} = (e_{\max} - e)/(e_{\max} - e_{\min}) \leq 0.90$, measured before the start of the regular cycles), five different average mean pressures ($50\,\mathrm{kPa} \leq p^{\mathrm{av}} \leq 300\,\mathrm{kPa}$) and four different average stress ratios ($0.5 \leq \eta^{\mathrm{av}} = q^{\mathrm{av}}/p^{\mathrm{av}} \leq 1.25$) have been tested. In four test series, one of these parameters has been varied, while the three remaining ones have been kept constant.

The measured development of permanent strain $\varepsilon^{\mathrm{acc}}$ with increasing number of cycles N is presented in the diagrams on the left-hand side of Fig. 2. Evidently, the residual strains $\varepsilon^{\mathrm{acc}}$ increase with increasing stress amplitude (Fig. 2a), decreasing initial density (Fig. 2c), and increasing average stress ratio (Fig. 2g). In case of a constant amplitude-pressure-ratio $\zeta = q^{\mathrm{ampl}}/p^{\mathrm{av}}$ similar accumulation curves are usually measured in tests with different average mean pressures (Fig. 2e).

The right-hand side of Fig. 2 contains diagrams in which the residual strain after certain numbers of cycles is plotted versus the parameter varied in the test series, i.e. against the strain amplitude $\bar{\varepsilon}^{\mathrm{ampl}}$, void ratio $\bar{e}$, average mean pressure p^{av} and average stress ratio η^{av}. $\bar{\varepsilon}^{\mathrm{ampl}}$ and $\bar{e}$ represent mean values of strain amplitude and void ratio up to the number of cycles under consideration. On the ordinate the residual strain has been divided by the functions f_{ampl} and/or f_e of the HCA model in order to remove any influence of slightly different strain amplitudes or void ratios. These functions are also evaluated with $\bar{\varepsilon}^{\mathrm{ampl}}$ and $\bar{e}$, which is indicated by the superposed bar $\bar{\square}$. Figure 2f shows that the intensity of accumulation decreases with increasing average mean pressure if a constant strain amplitude is considered. The other tendencies in Fig. 2b, d, h agree well with those in Fig. 2a, c, g.

The dependencies of the intensity of strain accumulation $\dot{\varepsilon}^{\mathrm{acc}}$ on strain amplitude, void ratio, average mean pressure and average stress ratio are described by the functions f_{ampl}, f_e, f_p and f_Y of the HCA model. The influence of the cyclic preloading history (i.e. of the number of cycles N in the simplest case of a cyclic loading with $\varepsilon^{\mathrm{ampl}} = \text{constant}$) is captured by the function $\dot{f}_N = \partial f_N/\partial N$. For the detailed equations of the HCA model the interested reader is referred to [10] or [19]. The parameters C_{ampl}, C_e, C_p, C_Y, C_{N1}, C_{N2} and C_{N3} used within the functions describing the intensity of accumulation can be calibrated "by hand" following the procedure described e.g. in [19,23]. Afterwards an optimization can be done by means of an element test program. The results of such simulations with the optimum set of parameters have been added as thick solid curves in Fig. 2. A good agreement between the measured data and the prediction by the HCA model can be concluded from Fig. 2.

Figure 3 presents the paths of accumulated deviatoric versus accumulated volumetric strain measured in the test series with a variaton of η^{av}. Evidently, the deviatoric portion of strain accumulation increases with growing η^{av}. Numerous similar test series have shown that a purely volumetric accumulation of strain occurs for isotropic average stresses ($\eta^{\mathrm{av}} = 0$), while a purely deviatoric one can be expected at the critical state line ($\eta^{\mathrm{av}} = M_{cc} = 6\sin\varphi_{cc}/(3 - \sin\varphi_{cc})$). This dependence is described by the flow rule of the HCA model with the parameter φ_{cc} ($\varphi_{cc} = 33.1°$ for KFS, see the predictions added as solid curves in Fig. 3). In contrast, the direction of accumulation is only marginally influenced by variations in stress amplitude, soil density and average mean pressure.

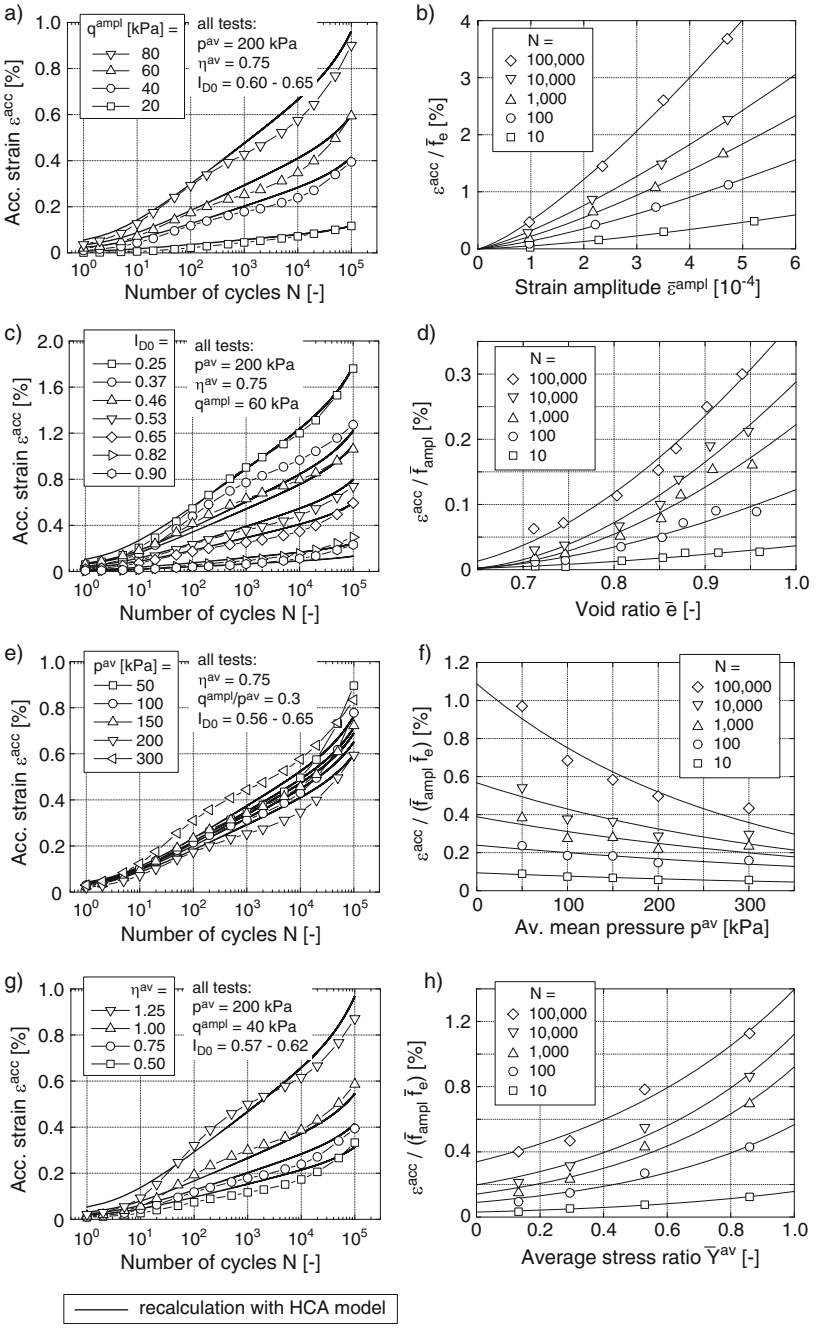

Fig. 2. Results of drained cyclic tests with different (a, b) stress amplitudes q^{ampl}, (c, d) initial relative densities I_{D0}, (e, f) average mean pressures p^{av} and (g, h) average stress ratios η^{av}

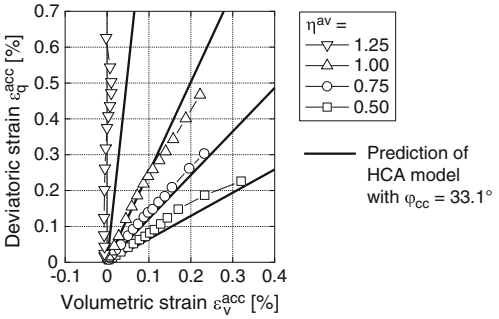

Fig. 3. $\varepsilon_q^{\mathrm{acc}} - \varepsilon_v^{\mathrm{acc}}$ strain paths measured in drained cyclic triaxial tests with different average stress ratios η^{av}; Description by the direction of accumulation (flow rule) in the HCA model

3 Grain Size Distribution Curve

An extensive laboratory testing program has been performed on special mixtures of a quartz sand with subangular grains, having linear grain size distribution curves with mean grain sizes in the range $0.1\,\mathrm{mm} \leq d_{50} \leq 6\,\mathrm{mm}$ and uniformity coefficients in the range $1.5 \leq C_u \leq 8$ [21–23]. These tests have been performed in the laboratory at RUB, using samples of 100 mm diameter and 200 mm height and a loading frequency of 1 Hz for the regular cycles. In Fig. 4 the residual strains after 10,000 cycles are plotted versus d_{50} or C_u, respectively. All specimens were medium dense and subjected to the same average and cyclic stresses. Figure 4 reveals that the residual strains are larger for sands with smaller mean grain sizes and higher uniformity coefficients. Also the shape of the strain accumulation curves $\varepsilon^{\mathrm{acc}}(N)$ depends on the granulometric properties [21,23], while the direction of accumulation is rarely affected [22]. In simulations with the HCA

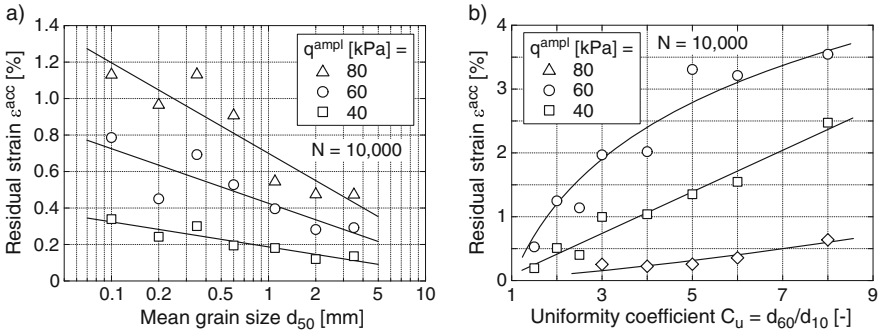

Fig. 4. Accumulated strain $\varepsilon^{\mathrm{acc}}$ after 10,000 cycles as a function of (a) mean grain size d_{50} and (b) uniformity coefficient C_u (all tests: $p^{\mathrm{av}} = 200\,\mathrm{kPa}$, $\eta^{\mathrm{av}} = 0.75$, medium dense samples)

model the influence of the grain size distribution curve is considered by chosing different sets of material constants.

For a simplified calibration of the parameters of the HCA model, correlations with the grain size distribution curve (mean grain size d_{50}, uniformity coefficient C_u) or index properties from simple laboratory tests (minimum void ratio $e_{\min}$) have been proposed [21–23].

4 Particle Characteristics

The influence of grain shape and surface roughness has been studied in drained cyclic triaxial tests on glass beads, natural sand and crushed sand. All three materials were tested with the same grain size distribution curve ($d_{50} = 0.6$ mm, $C_u = 1.5$). Each of the three materials has been tested with different initial relative densities I_{D0}, deviatoric stress amplitudes q^{ampl} and average stresses (p^{av}, η^{av}) [26]. The diagrams in Fig. 5 present the accumulated strain $\varepsilon^{\mathrm{acc}}$ after $N = 10^5$ cycles as a function of the stress amplitude q^{ampl} or average mean pressure p^{av}, respectively. While for glass beads and natural sand the residual strain grows faster than proportional with increasing stress amplitude, the opposite is true in the case of the crushed sand.

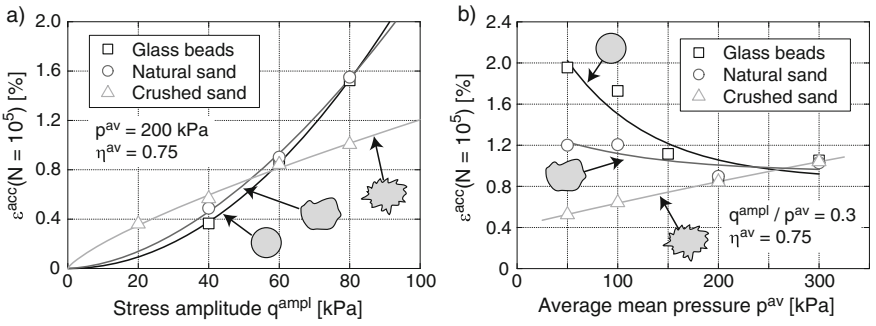

Fig. 5. Results from drained cyclic tests on medium dense samples of three materials with different grain shape: Accumulated strain $\varepsilon^{\mathrm{acc}}$ after $N = 10^5$ cycles as a function of (a) stress amplitude q^{ampl} and (b) average mean pressure p^{av}

The largest differences are evident in the series with different average mean pressures. The tests on glass beads showed a significant decrease of the residual strain with increasing values of p^{av}. Also the natural sand exhibited a moderate reduction. The opposite, i.e. a considerable increase of $\varepsilon^{\mathrm{acc}}$ with p^{av} was observed for the crushed sand. At low pressures ($p^{\mathrm{av}} = 50$ kPa) the rates of strain accumulation were much higher in the tests on the glass beads compared to the natural sand and in particular to the crushed sand. At higher pressures ($p^{\mathrm{av}} = 300$ kPa) no significant differences between the residual strains measured for the three different materials could be detected. This is probably due to the fact,

that larger contact forces lead to a flattening of the contact zones. Therefore, with increasing stresses, the shape of the contacts developing in the different materials converges. The original shape of the particles involved in the contact then becomes less important. At lower contact stresses, reorientations of the particles due to slipping and rotation are easier in the assemblies of round glass beads with their smooth surface than in the angular crushed sand with a distinct interlocking between adjacent grains.

5 Content of Non-cohesive Fines or Shell Fragments

The influence of a non-cohesive fines content on the cumulative deformations has been investigated in a study with drained cyclic tests on fine sands possessing different amounts of fines (grains with sizes $d < 0.063\,\text{mm}$), namely $FC = 0$, 11.3 and 19.6%. At grain sizes $d > 0.063\,\text{mm}$ the grain size distribution curves of all mixtures were parallel to each other ($C_u = 1.5$). The residual strains after $N = 10^5$ cycles measured for different initial relative densities and fines contents are compared in Fig. 6a. Evidently, for a given I_{D0} value larger residual strains are obtained for the mixtures with a higher content of non-cohesive fines.

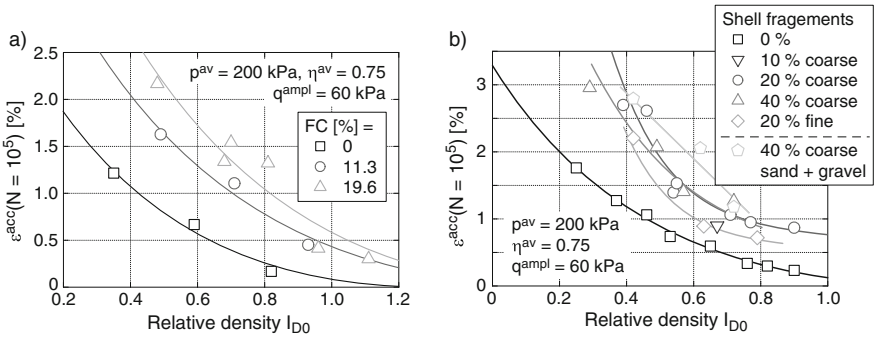

Fig. 6. Residual strain ε^{acc} after $N = 10^5$ cycles as a function of initial relative density I_{D0} in tests on (a) three fine sands with different amounts of non-cohesive fines and (b) mixtures of Karlsruhe fine sand with different percentage of shell fragments

In order to study the influence of a content of shell fragments, mixtures of Karlsruhe fine sand with different portions and sizes of North sea shell fragments (10, 20 or 40% coarse shell fragments with particle sizes $0.063 \leq d \leq 8\,\text{mm}$ or 20% fine shell fragments with $0.063 \leq d \leq 2\,\text{mm}$) have been subjected to a drained high-cyclic loading [27]. Figure 6b presents the measured residual strain after 10^5 cycles as a function of I_{D0}. For similar densities and identical average and cyclic stresses, the residual strain grows with increasing content of shell fragments. This is probably mainly attributed to the fact that the mixtures with higher contents of shell fragments are more well-graded, cf. [23]. This hypothesis

is supported by the fact that another mixture of KFS with 40% coarse sand and gravel particles delivered similar cumulative rates as the mixture containing 40% shell fragments (Fig. 6b). Both mixtures had identical grain size distribution curves. Furthermore, the mixture with 20% fine shell fragments, possessing a more uniform gradation, exhibited lower strain accumulation rates than the mixture with 20% coarse shell fragments. Therefore, the crushability and the platy particle shape of the shell fragments seem to be of secondary importance in this case.

In order to examine a possible breakage of the shell fragments during cyclic loading, a sieve analysis has been performed on a sample of the mixture with 40% shell fragments before and after a cyclic test. The grain size distribution curves determined before and after the test were practically identical, giving no hints for particle breakage. The shell fragments involved in the present study, primarily originating from cockles, seem to be too hard to allow for a significant amount of breakage under the applied average and cyclic loads, in particular when they are embedded into a fine sand matrix.

6 Sample Preparation Method

It is well known that the initial fabric, generated in the laboratory by the chosen sample preparation method, has a large influence on the behaviour of sand, in particular under undrained monotonic and cyclic loading [3,6,7,14,15,17]. Therefore, the influence has been investigated for a drained high-cyclic loading. The samples of KFS were prepared by the following eight methods, which are depicted by the schemes in Fig. 7:

- Air pluviation, where dry sand falls out of the outlet of a funnel
- Homogeneous dry sand rain over the whole cross section of the sample using a multiple sieve apparatus similar to the one proposed in [6]
- Air pluviation by means of a large sand spreader (diameter $d \approx 1$ m), usually applied for model testing at the IBF [28].
- Water pluviation, leading to rather low initial densities not exceeding $I_{D0} = 0.3$, with subsequent compaction by vibration applied with a shaking table (for densities $I_{D0} > 0.3$)
- Water pluviation with subsequent compaction by tapping of the mold using a rubber hammer
- Dry deposition in the loosest state with subsequent compaction by vibration applied with a shaking table
- Dry deposition in the loosest state with subsequent compaction by tapping of the mold using a rubber hammer
- Moist tamping in eight layers using the undercompaction method proposed in [4] with a water content of 10% and a degree of undercompaction of 5%. For samples with $I_{D0} > 0.8$ a constitution procedure analogous to the Proctor test has been alternatively used.

For each sample preparation method several drained cyclic triaxial tests with different relative densities but same average and cyclic stresses ($p^{av} = 200\,kPa$, $\eta^{av} = 0.75$, $q^{ampl} = 60\,kPa$) have been performed. The residual strains at the end of 10^5 cycles are given in Fig. 7 as a function of I_{D0}.

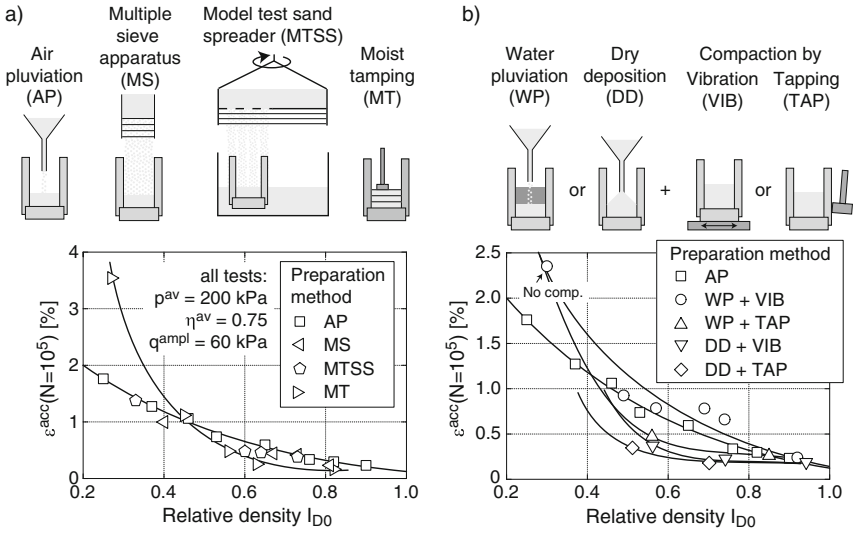

Fig. 7. Accumulated strain after 10^5 cycles versus initial relative density for various sample preparation methods

The samples prepared by the different dry pluviation techniques (AP, MS, MTSS) gave almost identical results (Fig. 7a). The conventional air pluviation technique (AP) and the procedure involving a multiple-sieve apparatus (MS), leading to a homogeneous sand rain over the whole sample cross section, seem thus to generate a similar initial fabric. The good agreement between the results for the conventional air-pluviated samples (AP) and those constituted by means of the model test sand spreader (MTSS) confirms that parameters (e.g. material constants of a constitutive model) obtained from conventional laboratory samples are representative for the sand in the model tests, i.e. may be regarded as appropriate for simulations of the model tests (see e.g. the FE re-calculations of small-scale model tests on OWPP foundations presented in [28] and [29]).

The diagram in Fig. 7b confirms that for I_{D0} = constant, water-pluviated samples compacted by vibration (WP + VIB) show similar cumulative strains than those constituted by air pluviation (AP). A compaction by tapping (WP + TAP) seems to lead to a fabric being more resistant to cumulative deformations than that of the vibrated samples, i.e. leading to lower accumulated strains. These differences are most striking for medium dense sand. In that range of

densities, even lower residual strains are generated in samples prepared by dry deposition in the loosest state followed by compaction (DD + VIB and DD + TAP, Fig. 7b).

Analyzing the data for moist tamping (MT) in Fig. 7a, it is a matter of density whether these samples deliver higher or lower intensities of strain accumulation compared to the air-pluviated specimens. The tamped samples show higher permanent strains in the loose state, but lower cumulative rates at medium density, leading to a considerably different shape of the $\varepsilon^{acc}(I_{D0})$ curve. Considering the different course of the strain accumulation curves $\varepsilon^{acc}(N)$ of the tamped and the pluviated samples, the deviations between both types of samples in a $\varepsilon^{acc} - I_{D0}$ diagram are additionally dependent on N.

Generally, the sample preparation method should be chosen in accordance with the assumed genesis of the sand deposit in situ.

7 Bedding Plane Orientation

The effect of the bedding plane orientation with respect to the polarization of the cyclic loading has been studied using a mold inclined by an angle α during the sample preparation by air pluviation (Fig. 8a). After preparation the samples were subjected to a cyclic loading in the axial direction. Results from tests with $\alpha = 0°$ (conventional samples) and $\alpha = 45°$ performed on medium dense KFS are presented in Fig. 8b. The data demonstrate that the influence of the bedding plane inclination α on the cumulative behaviour of KFS is rather small, probably due to the predominantly compact particles of this sand.

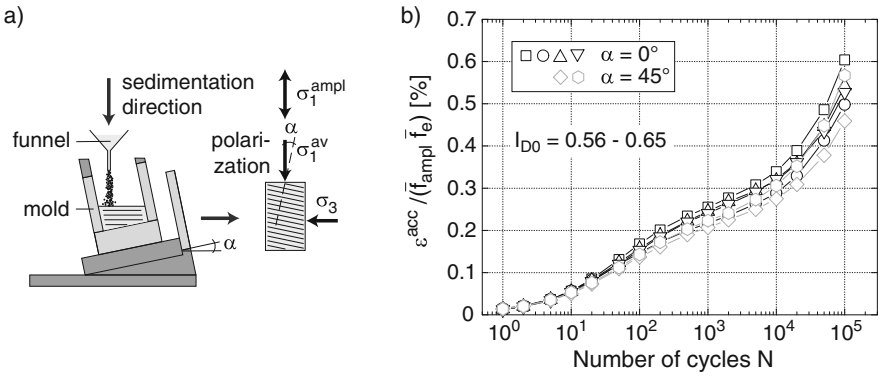

Fig. 8. Comparison of samples with bedding plane inclinations $\alpha = 0°$ and $\alpha = 45°$ subjected to a drained high-cyclic loading in the vertical direction

8 Sample Geometry and Dimensions

The influence of sample geometry and dimensions has been investigated in a series of tests on KFS. Five types of samples have been tested, four of them

being cylindrical and one cuboid-shaped (see the schemes in Fig. 9). In case of the cylindrical specimens, beside the IBF standard ($d = h = 100\,\text{mm}$) further 1:1 samples with smaller ($d = h = 50\,\text{mm}$) and larger size ($d = h = 150\,\text{mm}$) have been tested. Furthermore, also 2:1 samples ($d = 100\,\text{mm}$, $h = 200\,\text{mm}$) have been included in the testing program. The cuboid-shaped specimens measured $a \times b = 90 \times 90\,\text{mm}$ in cross section and $h = 180\,\text{mm}$ in height. They are further used for local strain measurements in Sect. 12.

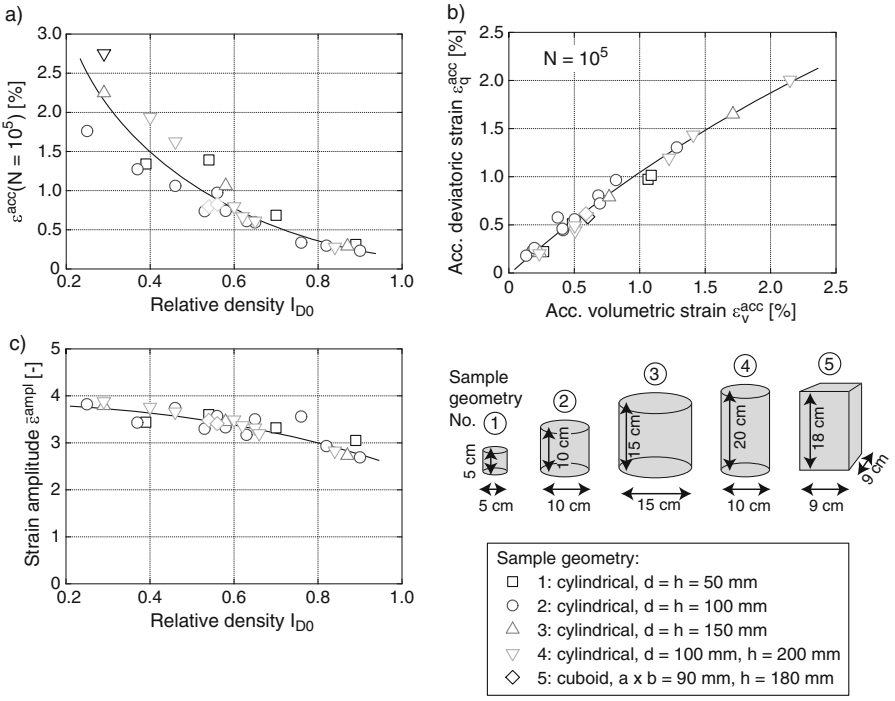

Fig. 9. Results from a test series with different sample geometries: (a) Accumulated strain ε^{acc} after 10^5 cycles versus initial relative density I_{D0}, (b) Accumulated deviatoric strain ε_q^{acc} versus accumulated volumetric strain ε_v^{acc} both measured at $N = 10^5$, (c) mean value of strain amplitudes $\bar{\varepsilon}^{ampl}$ over 10^5 cycles

Figure 9 presents the data from tests with the same average and cyclic stresses ($p^{av} = 200\,\text{kPa}$, $\eta^{av} = 0.75$, $q^{ampl} = 60\,\text{kPa}$) but different initial relative densities. For the cylindrical 2:1 and the cuboid-shaped samples only medium densities were tested, while a larger I_{D0} range was investigated for the three other types. The accumulated strain ε^{acc} after 10^5 cycles measured for the different types of samples were quite similar for medium to high densities, but showed stronger variations at lower densities, with higher residual strains for the larger samples ($d = h = 150\,\text{mm}$ and $d = 100\,\text{mm}$, $h = 200\,\text{mm}$), Fig. 9a. The reasons are not

clear so far. Since several years lay between the tests on the standard samples ($d = h = 100\,\text{mm}$) and those on all other types of samples, the differences could be caused by changes of the re-used test material (e.g. by abrasion) or by the different technicians preparing the samples (i.e. slightly different fabric). In contrast, the influence of the sample geometry and dimensions on the direction of strain accumulation (Fig. 9b) and on the strain amplitudes (Fig. 9c) is rather small in this case. The differences in $\bar{\varepsilon}^{\text{ampl}}$ may be larger for coarser granular materials, as demonstrated by another series of tests in [19].

9 Multiple Changes of Polarization

Based on multi-dimensional simple shear tests an earlier study documented in [18,20] demonstrated that a change of the polarization, i.e. the direction of the cycles in the strain space by 90° leads to a temporary increase of the rate of strain accumulation. These findings were later confirmed in [5], where also changes of the polarization ≠90° were tested. However, all tests in [5,18,20] were restricted to a single change of the polarization only. In order to study the effect of multiple polarization changes, a new test series on Karlsruhe fine sand has been conducted in the triaxial apparatus [25]. In all tests the cycles were superposed to an average stress with $p^{\text{av}} = 200\,\text{kPa}$ and $\eta^{\text{av}} = 0.5$.

Six different polarizations have been tested. The stress paths in the P-Q plane are shown in the scheme in Fig. 10a. The isometric variables $P = \sqrt{3}p$ and $Q = \sqrt{3/2}q$ [9] are advantageous in connection with studies on the influence of the polarization because the lengths of the stress paths and the angles between two polarizations are preserved when transferred from a principal stress coordinate system to the P-Q plane, in contrast to the p-q representation. In the present test series, two neighbored polarizations differed by an angle $\Delta\alpha_{PQ} = 30°$ in the P-Q plane. Polarizations 1 and 4 were parallel to the P- or Q-axis, respectively, i.e. they represent purely isotropic or purely deviatoric stress cycles. In order to achieve the stress paths depicted in Fig. 10a a simultaneous oscillation of the axial and the lateral effective stress was necessary. Due to the simultaneous σ'_1 and σ'_3 variation a relative low frequency of 0.01 Hz has been chosen for the regular cycles in all tests within this study. This implicates a lower maximum number of cycles compared to other test series presented herein.

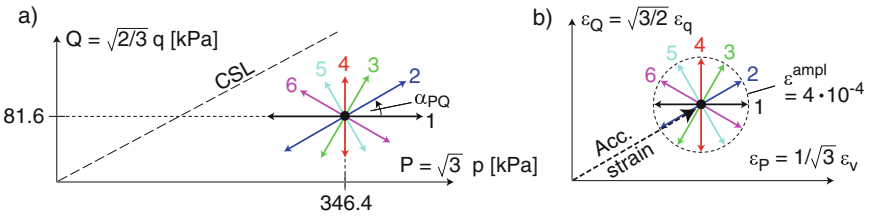

Fig. 10. Stress and strain paths in the tests with multiple polarization changes (CSL = critical state line)

The strain paths are shown schematically in a $\varepsilon_P - \varepsilon_Q$ diagram in Fig. 10b, using the isometric strain variables $\varepsilon_P = \varepsilon_v/\sqrt{3}$ and $\varepsilon_Q = \sqrt{3/2}\varepsilon_q$. The tests were performed stress-controlled. Based on preliminary tests the stress amplitudes have been chosen in order to achieve a strain amplitude $\varepsilon^{\mathrm{ampl}} = \sqrt{(\varepsilon_P^{\mathrm{ampl}})^2 + (\varepsilon_Q^{\mathrm{ampl}})^2} \approx 4 \cdot 10^{-4}$ for all six polarizations at a medium density $I_{D0} \approx 0.6$.

52 tests with initial relative densities in the range $0.42 \leq I_{D0} \leq 0.84$ have been performed, among them 41 with multiple polarization changes and 11 reference tests with a constant polarization throughout the test. The 20 different sequences applied in the tests with polarization changes are illustrated in Fig. 11. In case of sequences Nos. 1 to 5 the polarization was changed every 1000 cycles. All six polarizations were involved in the first four sequences while only purely isotropic and purely deviatoric stress cycles (polarizations 1 and 4) were alternatingly applied in the tests with the fifth sequence. The polarization was altered every 2500 cycles in case of sequences Nos. 6 to 16, while the polarization was kept constant for 5000 cycles in case of sequences Nos. 17 to 20. In all these tests a total number of at least 10,000 cycles has been applied. The reference tests were performed with 11,000 cycles along polarizations 1, 4 or 5.

The influence of the polarization with respect to the sedimentation direction can be studied based on the first 1,000 cycles of each test, i.e. the data recorded prior to the first change of the polarization. Figure 12a demonstrates that the residual strain after 1,000 cycles is only marginally affected by the polarization. Based on this knowledge, next the influence of *changes* of the polarization can be studied.

Figure 12b presents the curves of accumulated strain $\varepsilon^{\mathrm{acc}}(N)$ during the tests with 11 or 12 packages of cycles, i.e. 10 or 11 polarization changes. For comparison purpose, the data from tests with a constant polarization (1D tests) performed on samples with similar initial density have been added in Fig. 12b. The differences between the curves $\varepsilon^{\mathrm{acc}}(N)$ obtained in the individual tests are primarily due to the variations in the initial densities. A temporary increase of the rate of strain accumulation usually occurred due to the first change of the polarization only. All subsequent alterations of the cyclic loading direction had only a moderate impact on the further course of the curves $\varepsilon^{\mathrm{acc}}(N)$.

In Fig. 12c the residual strain after 10,000 cycles is given as a function of initial relative density. The different symbols distinguish between different numbers of polarization changes during the cyclic loading. The data do hardly show any clear differences between the tests with 9 polarization changes and those with constant polarization. The same applies to the tests with a single change. Surprisingly, the effect is more pronounced in case of the tests with three such alterations of polarization. Almost independent of initial density, the tests with three polarization changes delivered an about $\Delta\varepsilon^{\mathrm{acc}} = 0.1$ to 0.2% larger residual strain than those with a lower or higher number of α_{PQ} alterations.

The $\varepsilon_q^{\mathrm{acc}} - \varepsilon_v^{\mathrm{acc}}$ data after $N = 10{,}000$ cycles shown in Fig. 12d do not show any noticeable effect of the number of polarization changes conducted during these cycles. Also the $\varepsilon_q^{\mathrm{acc}} - \varepsilon_v^{\mathrm{acc}}$ strain paths measured in the individual tests

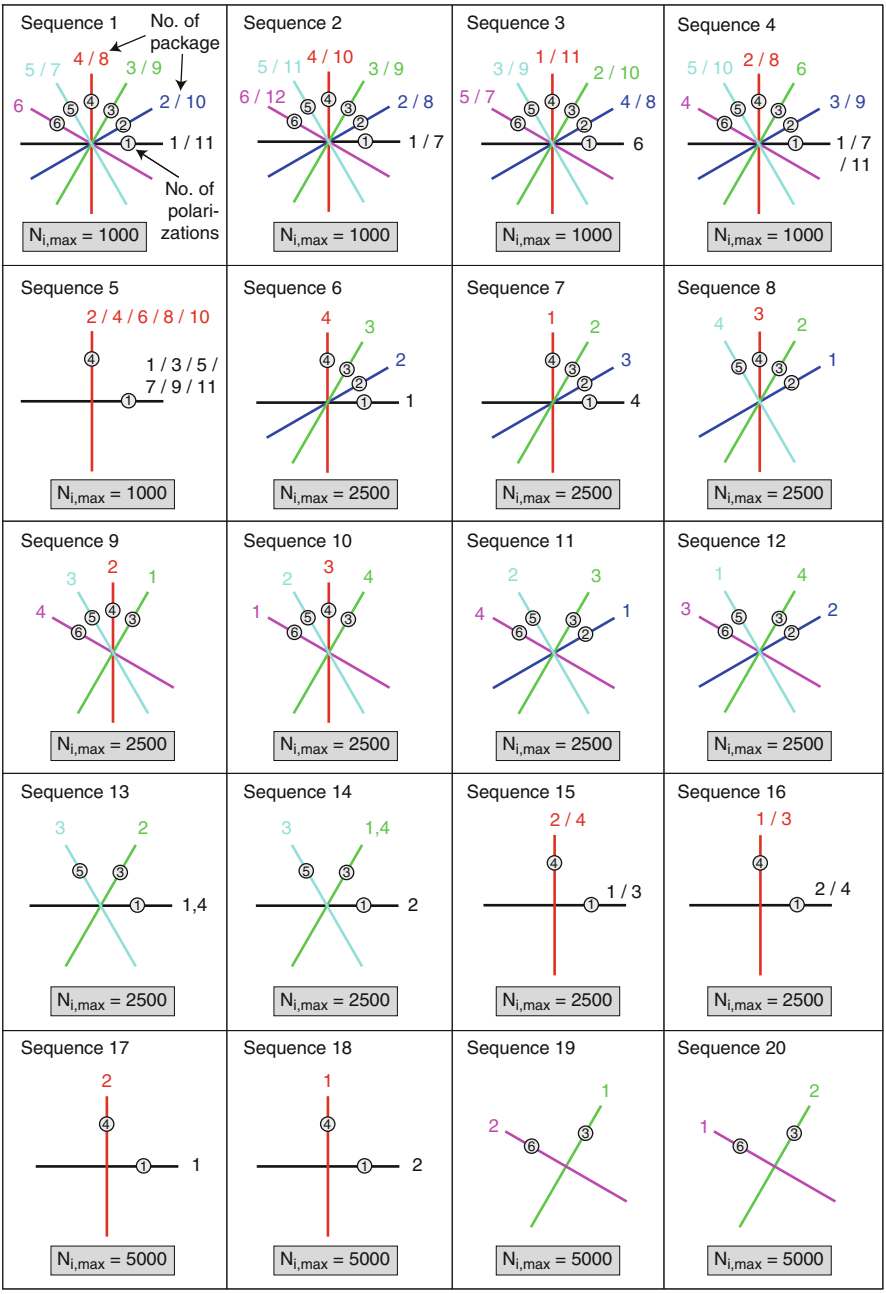

Fig. 11. Sequences of polarizations applied in the tests ($N_{i,\max}$ = number of cycles in each package with a certain polarization)

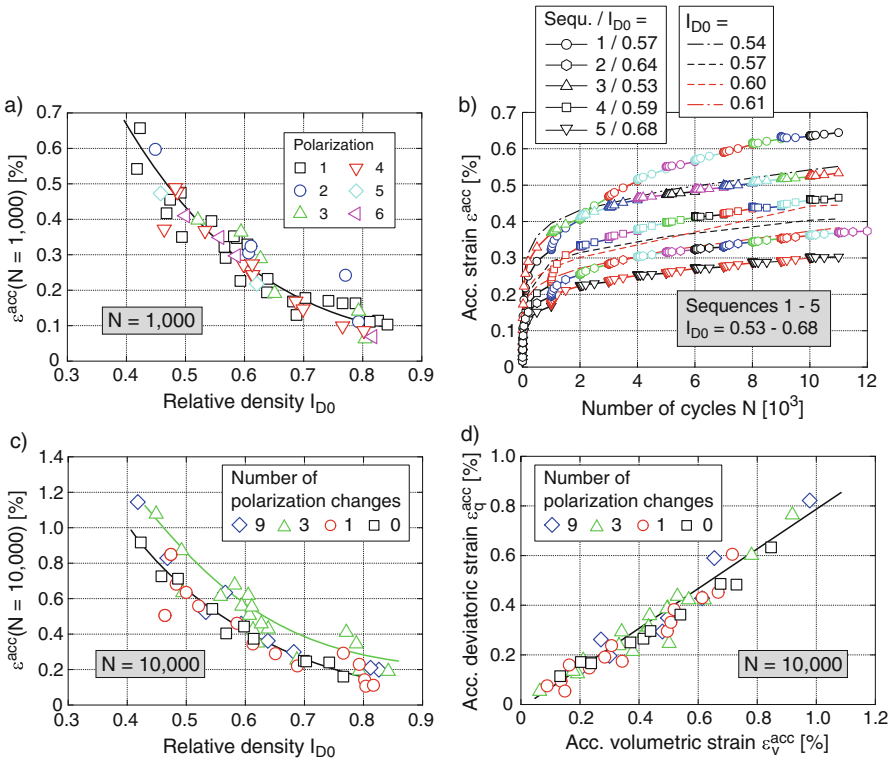

Fig. 12. (a) Accumulated strain $\varepsilon^{\mathrm{acc}}$ after 1000 cycles as a function of initial relative density I_{D0}, (b) Development of accumulated strain $\varepsilon^{\mathrm{acc}}(N)$ in five tests with different sequences of polarizations and in the corresponding reference tests with constant polarization, (c) Accumulated strain $\varepsilon^{\mathrm{acc}}$ after 10,000 cycles as a function of initial relative density I_{D0}, (d) Accumulated deviatoric strain $\varepsilon_q^{\mathrm{acc}}$ as a function of accumulated volumetric strain $\varepsilon_v^{\mathrm{acc}}$ after 10,000 cycles

confirm that the direction of strain accumulation is not altered by the multiple changes of the direction of the cycles.

Based on Fig. 12c it can be concluded that the influence of multiple polarization changes on the final residual strain may be regarded as less important than previously thought, based on the experiments presented in [20] or [5]. It seems relevant for the first change of the polarization only and has only a moderate effect on the residual strain after a larger number of cycles. Thus the factor f_π of the HCA model, describing the effect of polarization changes, could possibly be omitted. A moderate increase of the rate of strain accumulation (e.g. via a 20% increase of parameter C_{N1}) for problems with multiple polarization changes could be sufficient for practical purposes.

It should be kept in mind, however, that although the effect of polarization changes may be of minor importance on the element test level, it can be of

relevance for foundation systems. For example, in case of piles (e.g. [1,11,12]) the change of the cyclic loading direction goes along with a change of the region of soil involved in strain accumulation or stress relaxation. Zones with low cumulative effects before the polarization change may be subjected to a large cyclic impact afterwards, and vice versa. Such influence of polarization changes on the foundation level can be studied in FE simulations with the HCA model.

10 Bundling of Cycles with Similar Amplitudes

In many practical problems the amplitude changes from cycle to cycle. In order to handle such random cyclic loading with a HCA model the cycles with similar amplitudes have to be grouped into packages. The packages are then treated sequentially. Such bundling is only allowed if the original random sequence of amplitudes generates a similar final residual strain as the same cycles when ordered into packages. A respective examination was the purpose of the tests presented in this section. All tests were performed on medium dense KFS with an average stress of $p^{\mathrm{av}} = 200\,\mathrm{kPa}$ and $\eta^{\mathrm{av}} = 0.75$. Each of the four stress amplitudes $q^{\mathrm{ampl}} = 20$, 40, 60 and 80 kPa was applied with 12,500 cycles. The total number of cycles was thus 50,000 in all tests. The sequence of the stress amplitudes has been varied, as shown by the schemes in Fig. 13a.

Figure 13b presents the measured strain accumulation curves for the eight different signals shown in Fig. 13a. In order to purify the data from the influence of the slightly different initial densities, the residual strain $\varepsilon^{\mathrm{acc}}$ has been divided by the void ratio function f_e of the HCA model, which was evaluated with the initial void ratio e_0 of a sample. Obviously, all tests with signals of types 1 to 4, i.e. with a frequently changing amplitude, deliver a similar residual strain $\varepsilon^{\mathrm{acc}}/f_e(e_0)$ after 50,000 cycles, irrespective of the order of the amplitudes. The tests with cycles grouped into four or eight packages (types 5 to 8) lead to even somewhat larger residual strains at the end of the test (Fig. 13b). This is also evident in Fig. 13c where the final residual strain after 50,000 cycles has been plotted versus I_{D0}. It can be concluded that the bundling of cycles with frequently changing amplitudes into a limited number of packages with constant amplitudes leads to a slight overestimation of the residual deformations, i.e. the procedure is conservative.

11 Monotonic Loading Between Bundles of Cycles (Loss of Cyclic Preloading Memory)

This test series [24] was originally dedicated to the question if the HCA model parameters can be calibrated from multi-stage tests, i.e. tests with a subsequent application of packages of cycles at various average stresses and with different stress amplitudes. Such multi-stage tests were thought to have the potential to significantly reduce the experimental effort necessary for the calibration of a full set of HCA model parameters. However, as demonstrated in the following, the test results revealed an effect not captured by the HCA model yet.

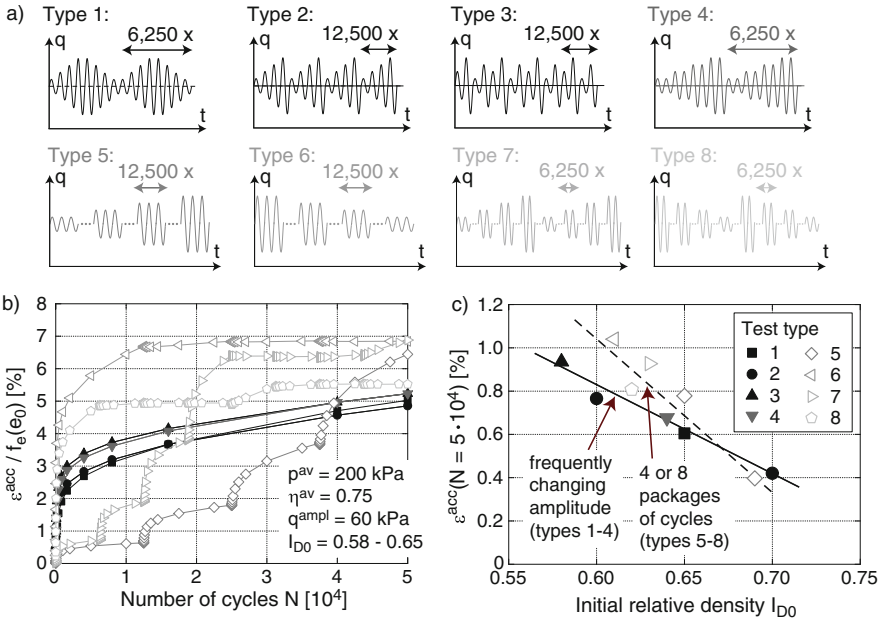

Fig. 13. Comparison of tests with frequently changing amplitude and tests with packages of cycles: (a) tested cyclic load signals, (b) accumulated strain ε^{acc} as a function of the number of cycles N, (c) residual strain after 50,000 cycles versus initial relative density I_{D0}

Medium dense samples of a natural fine sand ($d_{50} = 0.10\,\text{mm}$, $C_u = 1.6$) taken near-shore in Cuxhaven, Germany have been tested in this series. The HCA model parameters of this sand had been already calibrated from 17 single-stage drained cyclic triaxial tests with different amplitudes, densities and average stresses [28].

The results from two of the new multi-stage tests are presented in Fig. 14. Figure 14a shows the development of accumulated strain ε^{acc} with increasing number of cycles N in a test with cycles applied at a constant average stress ($p^{av} = 200\,\text{kPa}$, $\eta^{av} = 0.75$). The four packages with 25,000 cycles each and stress amplitudes $q^{ampl} = 20$, 40, 60 and 80 kPa were applied in ascending order. The measured development of residual strain with N agrees well with similar test series in the literature [2,13,18]. $\varepsilon^{acc}(N)$ data stemming from a recalculation of this test using the HCA model with the parameters calibrated from the 17 single-stage tests are shown as the thick solid curve in Fig. 14a. Due to its preloading variable g^A the HCA model is able to reproduce well the experimental data.

In the multi-stage test presented in Fig. 14b the average stress ratio has been increased between the successive packages of cycles, keeping the average mean pressure constant ($p^{av} = 200\,\text{kPa}$). Each of the five packages comprised 25,000 cycles with a stress amplitude $q^{ampl} = 60\,\text{kPa}$. The $\varepsilon^{acc}(N)$ curve in Fig. 14b

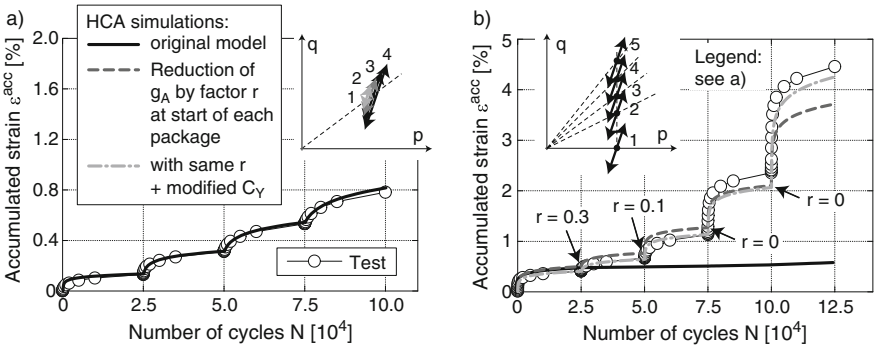

Fig. 14. Accumulation curves $\varepsilon^{\mathrm{acc}}(N)$ measured in the multi-stage tests with packages of cycles applied with different amplitudes or at different average stresses

exhibits an increase of the rate of strain accumulation at the beginning of each new package of cycles. The results of a simulation of this test with the HCA model using the parameters calibrated from the single-stage tests have been added as the thick solid curve in Fig. 14b. Evidently, the strain accumulation rates measured in the later packages of this test are significantly underestimated by the HCA model. This is in contrast to simulations of the single-stage tests, where the stress ratio-dependence experimentally observed could be adequately reproduced. Therefore, the differences between the experimental results and the model prediction apparent in Fig. 14b must be due to an effect not captured by the HCA model yet.

A drained cyclic loading leads to subtile changes in the orientations of the grains or grain contact normals, usually rendering the sand fabric more resistant to the subsequent cycles, i.e. leading to an adaption of the fabric to the actual cyclic loading and thus to a reduction of the strain accumulation rate $\dot{\varepsilon}^{\mathrm{acc}}$ with increasing number of cycles. In the HCA model this is phenomenologically captured by the preloading variable g^A. In the multi-stage test presented in Fig. 14b the change of the average stress between two succeeding packages of cycles represents a monotonic loading. It is likely that re-orientations of the grains caused by this monotonic loading erase some parts or the whole memory of the sand regarding the preceding cyclic loading. After sufficiently large monotonic strains the cumulative behaviour of the sand sample is probably similar to that of a freshly pluviated one, because the cyclic preloading history has been completely forgotten. In the context of the HCA model this means that the preloading variable g^A is reduced or even completely erased (to $g^A = 0$) by a monotonic loading. This effect has not been considered in calculations with the HCA model so far, i.e. the preloading variable g^A has been assumed to increase continuously only.

A better prediction of the experimental data in Fig. 14b (thick dashed curve) can be indeed achieved if g^A is reduced by a certain factor r at the start of each subsequent package. $r = 1$ means that the preloading variable remains unchanged and $r = 0$ corresponds to a total loss of the cyclic preloading memory. The r

values necessary for a satisfying reproduction of the test data are provided in Fig. 14b. A complete loss of memory can be concluded from the parameter $r = 0$ obtained for the packages applied at higher stress ratios. An almost perfect agreement with the test data can be achieved if additionally the parameter C_Y of the function f_Y, originally calibrated from the 17 single-stage tests, is slightly increased (thick dot-dashed curve in Fig. 14b). Based on the data from all tests within this series, it has been demonstrated in [24] that r correlates with the strain occurring during the monotonic loading phases. A more detailed experimental investigation of this effect followed by an incorporation in simulations with the HCA model is planned for the future.

The (partial) loss of the cyclic preloading memory due to monotonic loading may be of great practical relevance for foundations subjected to a cyclic loading with varying amplitudes and average stresses. Furthermore, a foundation is usually subjected to a monotonic loading during the construction phase caused by the own weight of the structure. This monotonic loading could partly or fully erase the memory of a cyclic loading history of the subsoil, probably leading to larger cumulative deformations during a subsequent cyclic loading of the foundations. Therefore, the conservative assumption $g_0^A = 0$ for the initial state in predictions with the HCA model, usually made because the cyclic preloading of the in situ soil is unknown and no suitable determination method is available yet, may be not as far from reality as previously thought. Beside that, the observed effect could be utilized for a reduction of the number of cyclic tests necessary for a calibration of the HCA model parameters. If a sample already tested under a certain cyclic loading condition can be reset to a state with $g_0^A = 0$ (similar to a freshly pluviated sample), simply by applying a monotonic loading, several average stresses or amplitudes could be tested in succession on a single sample.

12 Multi-dimensional Cyclic Loading

Earlier test series [18,20] had shown that two-dimensional (2D) stress or strain paths applied in a cyclic DSS or triaxial device deliver higher cumulative strains than 1D paths of similar span [20]. In the HCA model this is considered by a special tensorial definition of a multidimensional strain amplitude for (up to) 6D convex strain paths [9]. A scalar value of the strain amplitude $\varepsilon^{\mathrm{ampl}}$ is obtained from a procedure involving multiple projections of the original strain loop. As an example, projections from 3D to 1D are shown in Fig. 15. The projection is done in the direction of a line connecting the two points of the strain path with the largest distance in that direction. The (up to 6) values of maximum distance and the corresponding vectors describing the projection direction are finally used for calculating $\varepsilon^{\mathrm{ampl}}$. For details the interested reader is referred to [9]. The amplitude definition of the HCA model was only confirmed for 1D and 2D paths so far [18,20]. The experimental program described in this section has been performed with the aim of a validation for 1D to 4D paths. 4D paths mean an independent variation of four of the six components of the stress or strain tensor.

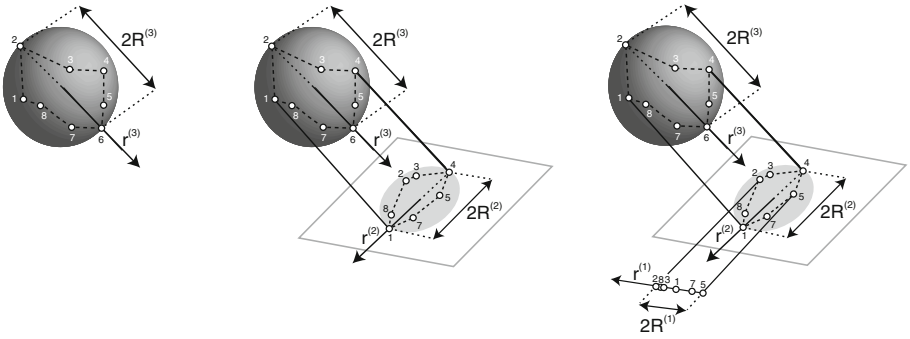

Fig. 15. Schemes showing the projections of a strain loop from 3D to 2D and from 2D to 1D for the determination of strain amplitude $\varepsilon^{\text{ampl}}$ according to the procedure described in [9]

The drained cyclic tests have been performed in three different types of test devices, using three different sample geometries and two different saturation conditions. 64 tests were conducted in a cyclic triaxial device as it has been used for most of the studies reported earlier in this paper (see the scheme in Fig. 1). Full cylinder samples (diameter $d = 100\,\text{mm}$, height $h = 200\,\text{mm}$, see a photo in Fig. 16a) have been used in these tests. 30 additional tests were performed in a hollow cylinder triaxial device (Fig. 16c). The samples had an outer diameter $d_a = 100\,\text{mm}$, an inner diameter $d_i = 60\,\text{mm}$ and a height $h = 200\,\text{mm}$. The volume changes of both the full and the hollow cylinder samples were measured via the pore water. Thus, the samples were tested fully water-saturated.

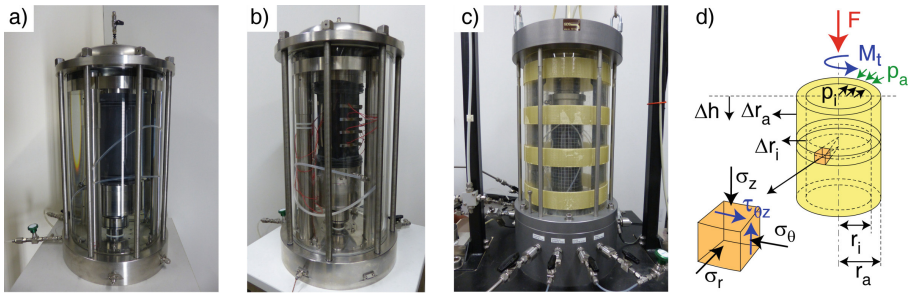

Fig. 16. Three types of devices used in the present study: (a) cyclic triaxial device with water-saturated full cylinder samples, (b) cyclic triaxial device with local strain measurements using LDTs on dry cuboid-shaped samples, (c) hollow cylinder device, (d) external loads and stresses acting on an element of soil in the hollow cylinder test

The application of 2D to 4D stress paths necessitates the cyclic variation of cell pressure, which can lead to membrane penetration effects [8,16]. These and

other sources of errors of global deformation measurements (e.g. system compliance, bedding error) can be avoided by applying local strain measurements. Therefore, for comparison purpose 26 further tests have been performed in a cyclic triaxial device similar to that shown in Fig. 1, but with local measurements of deformation on cuboid-shaped samples ($a \times b = 90\,\text{mm}$, $h = 180\,\text{mm}$). LDTs, i.e. strips of stainless steel equipped with strain gauges (Fig. 16b) were applied for that purpose. The cuboid-shaped samples were tested in the dry condition and without water in the pressure cell, in order to guarantee the long-term stability of the LDT measurements. The cell air pressure was kept constant to maintain a constant temperature in the cell, which is necessary for reliable LDT measurements. The cyclic variation of lateral effective stress was realized by an oscillation of pore air pressure.

In the triaxial devices (Fig. 16a, b) 1D stress paths with different inclinations in the P-Q plane and 2D stress paths can be applied by a simultaneous cyclic variation of effective axial stress (applied via the load piston) and effective lateral stress (applied as a cyclic variation of cell or pore pressure). 3D and 4D paths can be tested in the hollow cylinder device only. The independent cyclic variation of vertical force F, torsional moment M_T, outer cell pressure p_a and inner cell pressure p_i (Fig. 16d) allows independent oscillations of three normal stresses (σ_z in vertical, σ_r in radial and σ_θ in circumferential direction) and one shear stress component $\tau_{\theta z}$. These four stresses can be converted to three principal stresses σ_1, σ_2 and σ_3 by means of a rotation of the coordinate system by the angle α.

Air-pluviated samples of Karlsruhe fine sand have been used in all tests of this series. The samples have been prepared with two different initial relative densities ($I_{D0} \approx 0.40$ and 0.70). In all tests $N = 10.000$ regular cycles were applied at an average stress with $p^{\text{av}} = 200\,\text{kPa}$ and $\eta^{\text{av}} = 0.50$, using a loading frequency of $f = 0.02\,\text{Hz}$.

In the cyclic triaxial tests on water-saturated cylindrical and on dry cuboid-shaped samples 1D, 2D elliptical and 2D circular stress paths in the P-Q plane have been applied. All stress paths had a sufficient distance to the failure lines. For the 1D stress paths the left-hand side of Table 1 specifies the tested spans (lengths, double amplitudes) l_{PQ} and the inclinations (polarizations) α_{PQ} in the P-Q plane. A polarization $\alpha_{PQ} = 54.75°$ means a conventional cyclic axial loading at constant lateral effective stress. The dots in the table indicate that spans between $l_{PQ} = 60\,\text{kPa}$ and $l_{PQ} = 200\,\text{kPa}$ were tested in steps of $\Delta l_{PQ} = 10\,\text{kPa}$. For 2D stress paths the spans a_{PQ} and b_{PQ} in two orthogonal axes and the orientation α_{PQ} of the longer axis are given on the right-hand side of Table 1. For circular 2D stress paths $a_{PQ} = b_{PQ} = r_{PQ}$ holds. A polarization α_{PQ} cannot be specified for circular paths.

The program of the tests in the hollow cylinder device is shown in Table 2. The first test represents a reference test. It has been performed in analogy to the circular 2D stress paths applied in the cyclic triaxial tests with a radius $r_{PQ} = 40\,\text{kPa}$ in the P-Q plane. Such stress loop is achieved by a cyclic variation of the vertical and the radial stress with the amplitudes $\sigma_z^{\text{ampl}} = 40\,\text{kPa}$ and $\sigma_r^{\text{ampl}} = 28.28\,\text{kPa}$. These amplitudes have been kept constant within the whole

Table 1. Program of the cyclic triaxial tests with 1D or 2D stress paths

Dimension	Polarization α_{PQ} [°]	Span l_{PQ} [kPa]
1D	54.75	60.00
1D	54.75	70.00
1D	...	...
1D	54.75	200.00
1D	0	80.00
1D	45	80.00
1D	90	80.00
1D	135	80.00

Dimension	Polarization α_{PQ} [°]	Span a_{PQ} [kPa]	Span b_{PQ} [kPa]
2D	-	28.28	28.28
2D	-	40.00	40.00
2D	-	60.00	60.00
2D	-	80.00	80.00
2D	0	35.78	17.78
2D	0	80.00	40.00
2D	45	80.00	40.00
2D	90	80.00	40.00
2D	135	80.00	40.00

Table 2. Program of the cyclic hollow cylinder tests with 2D, 3D and 4D stress paths

No.	Dim.	Stress amplitudes				Phase shift			
		σ_z^{ampl} [kPa]	σ_r^{ampl} [kPa]	σ_θ^{ampl} [kPa]	$\tau_{\theta z}^{ampl}$ [kPa]	ϕ_{σ_z} [°]	ϕ_{σ_r} [°]	ϕ_{σ_θ} [°]	$\phi_{\tau_{\theta z}}$ [°]
1	2D	40.00	28.28	28.28	0.00	35.26	125.26	125.26	0.00
2	3D	40.00	28.28	56.56	0.00	35.26	125.26	125.26	0.00
3	3D	40.00	28.28	28.28	28.28	35.26	125.26	125.26	0.00
4	4D	40.00	28.28	56.56	28.28	35.26	125.26	62.63	62.63
5	4D	40.00	28.28	56.56	28.28	35.26	125.26	125.26	125.26

test series. By a cyclic variation of the two remaining stress components σ_θ and $\tau_{\theta z}$ with the amplitudes σ_θ^{ampl} and $\tau_{\theta z}^{ampl}$ and by chosing different values of phase shift ϕ between the different stress components up to 4D stress paths could be investigated. The loading frequency was the same for all four stress components.

Figure 17 compares data from the triaxial tests performed on either the fully water-saturated full cylinder samples with global strain measurements (left column of diagrams) or the dry cuboid-shaped samples with local strain measurements (right column). In both cases results for two different 1D stress paths with inclinations α_{PQ} of either $-45°$ or $45°$, two elliptical 2D paths with different inclinations of the larger axis ($\alpha_{PQ} = 0°$ and $90°$) and a circular 2D path are shown. A comparison of the diagrams in the first and second row of Fig. 17 reveals that circular stress paths in the P-Q plane cause elliptical strain paths in the $\varepsilon_P - \varepsilon_Q$ diagram, with a longer axis in the deviatoric direction. The strain amplitudes given as a function of the number of cycles in Fig. 17c, g have been derived following the procedure described in [9] and illustrated in

Fig. 15. According to that definition, the strain amplitude increases with increasing area encompassed by the strain path in the $\varepsilon_P - \varepsilon_Q$ diagram. The smallest strain amplitudes are obtained for the 1D stress path with $\alpha_{PQ} = 45°$, while the circular 2D stress path delivers the highest values. Evidently, for the same stress paths, the strain amplitudes obtained from the local strain measurements on dry cuboid-shaped samples (Fig. 17g) are slightly smaller than those derived from the global deformation records in case of fully water-saturated cylindrical samples (Fig. 17c). The differences are probably mainly caused by the different states of saturation rather than by the differences in the method of strain measurement or sample geometry. The higher stiffness of KFS in the dry condition compared to the water-saturated state has been already observed in previous experimental studies, using cylindrical samples and global measurements in all tests [19]. A comparison of the diagrams in Fig. 17c, g and d, h reveals that for both types of samples and saturation conditions, higher strain amplitudes lead to larger cumulative strains.

A comparison of the results from the tests with the same circular stress paths applied on the three types of samples is shown on the left-hand side of Fig. 18. The data confirms the smaller strain amplitudes for the dry cuboid-shaped samples compared to the water-saturated full cylinder samples (Fig. 18c). The highest strain amplitudes were recorded for the hollow cylinder samples, however. Again, larger strain amplitudes (Fig. 18c) lead to larger strain accumulation rates (Fig. 18d), at least at $N > 100$.

The results of the five different types of hollow cylinder tests listed in Table 2, with 2D, 3D or 4D stress paths are provided on the right-hand side of Fig. 18. The smallest strain amplitudes and cumulative strains were obtained for the 2D stress path, while the largest values resulted from the 4D one. Thus, with increasing dimensionality of the stress path, both the strain amplitudes $\varepsilon^{\mathrm{ampl}}$ and the cumulative strains $\varepsilon^{\mathrm{acc}}$ grow.

Finally, in Fig. 19 the cumulative strains $\varepsilon^{\mathrm{acc}}$ after 10,000 cycles from all 120 tests are given as a function of the strain amplitude $\bar{\varepsilon}^{\mathrm{ampl}}$ of that test. The strain amplitude is calculated as a mean value over 10,000 cycles. The diagram contains data for the two different relative densities $I_{D0} \approx 0.40$ and $I_{D0} \approx 0.70$. For a certain density, the $\varepsilon^{\mathrm{acc}} - \bar{\varepsilon}^{\mathrm{ampl}}$ data for the different types of samples, saturation conditions and dimensionality of the stress or strain path (1D up to 4D) lie on a unique curve. Thus, the definition of the strain amplitude according to Niemunis [9] allows the description of the $\varepsilon^{\mathrm{acc}} - \bar{\varepsilon}^{\mathrm{ampl}}$ relationship by a single function. In the present case, the function $\varepsilon^{\mathrm{acc}} \sim (\bar{\varepsilon}^{\mathrm{ampl}})^n$ has been fitted to the data, leading to exponents $n = 1.40$ for $I_{D0} = 0.40$ and $n = 1.48$ for $I_{D0} = 0.70$. Based on Fig. 19 the amplitude definition used in the HCA model can be seen as validated for strain paths from 1D to 4D.

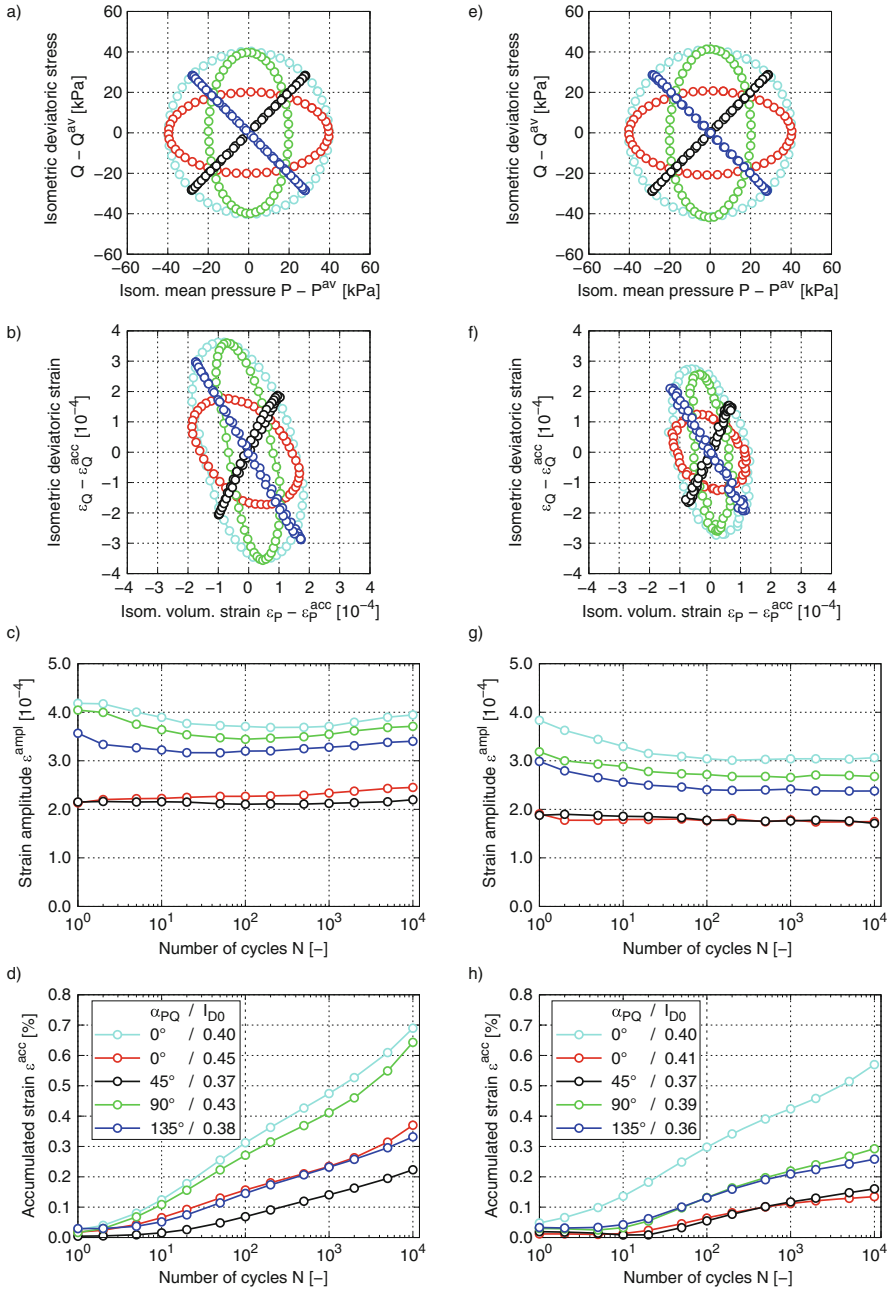

Fig. 17. Selected cyclic triaxial tests on fully water-saturated full cylinder samples (left-hand side) and dry cuboid-shaped samples (right-hand side): (a, e) P-Q stress paths, (b, f) $\varepsilon_P - \varepsilon_Q$ strain paths at $N = 10{,}000$, (c, g) development of strain amplitude $\varepsilon^{\mathrm{ampl}}$ and (d, h) accumulated strain $\varepsilon^{\mathrm{acc}}$ with increasing number of cycles N in tests on medium dense samples ($I_{D0} \approx 0.40$)

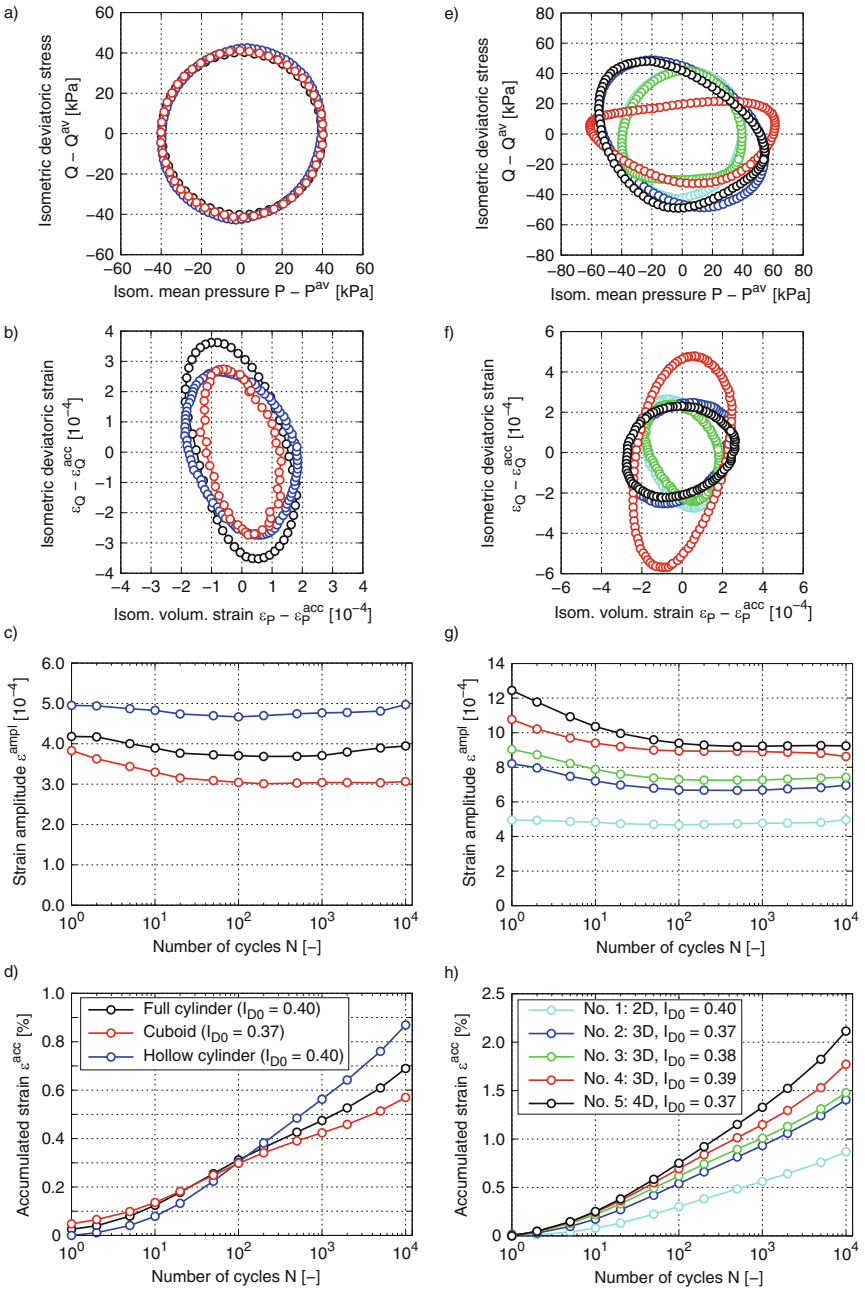

Fig. 18. Left-hand side: Comparison of results from the three types of tests for a circular 2D stress path (hollow cylinder test No. 1 in Table 2); Right-hand side: Results from hollow cylinder tests Nos. 1 to 5 with 2D to 4D stress paths; (a, e) P-Q stress paths, (b, f) ε_P-ε_Q strain paths at $N = 10{,}000$, (c, g) development of strain amplitude $\varepsilon^{\mathrm{ampl}}$ and (d, h) accumulated strain $\varepsilon^{\mathrm{acc}}$ with increasing number of cycles N in tests on medium dense samples ($I_{D0} \approx 0.40$)

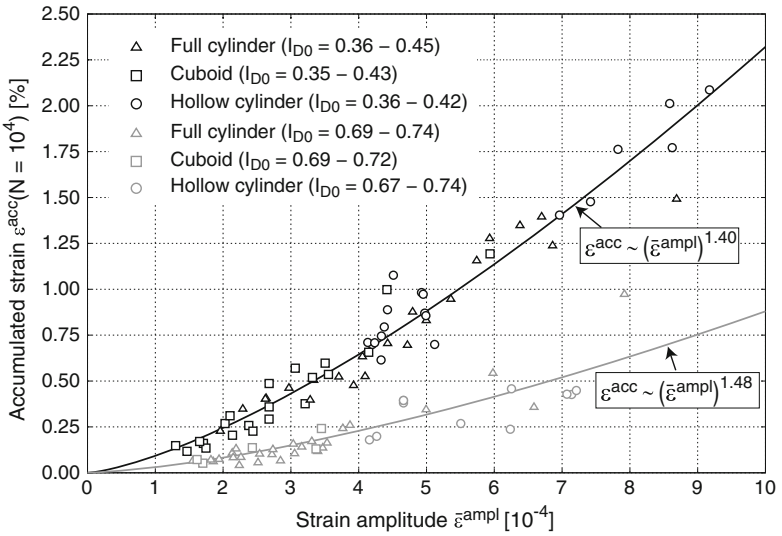

Fig. 19. Compilation of the data of all 120 cyclic tests with 1D to 4D stress paths, performed on either fully water-saturated full cylinder samples, dry cuboid-shaped samples with local strain measurements or water-saturated hollow cylinder samples: Accumulated strain ε^{acc} after 10,000 cycles as a function of the strain amplitude $\bar{\varepsilon}^{ampl}$ for relative densities $I_{D0} \approx 0.40$ and $I_{D0} \approx 0.70$. The strain amplitude has been evaluated by applying the procedure described in [9]. $\bar{\varepsilon}^{ampl}$ is a mean value over 10,000 cycles.

13 Summary, Conclusions and Outlook

The rates of strain accumulation in sand under high-cyclic loading grow with increasing stress or strain amplitude, decreasing density and increasing average stress ratio. At similar values of relative density, average stress and stress amplitude, finer and more well-graded clean sands show higher cumulative strains. A content of non-cohesive fines or shell fragments up to 20% further increases the rates of strain accumulation. Tests on glass beads, natural sand and crushed sand demonstrate that the influence of grain shape depends on stress level. At low pressures, materials with round particles show considerable larger strain accumulation rates than those with angular grains. At higher pressures, the particle shape seems to become rather irrelevant.

A considerable influence of the sample preparation method, in particular at medium density, has been observed in a series where the samples have been constituted either by air pluviation, water pluviation or moist tamping and compacted by vibration or tapping. At medium density air pluviated samples and water-pluviated samples compacted by vibration showed the largest cumulative rates, while the samples compacted by tapping or prepared by moist tamping turned out to be the most resistant ones. In tests on air-pluviated samples of a fine sand the effect of the bedding plane orientation was found to be of minor

importance. The influence of the sample geometry was rather small for medium dense to dense fine sand, but some differences in the cumulative strains for loose samples need further investigations.

The effect of multiple polarization changes has been found less significant as assumed based on previous studies with only a single change of the direction of the cycles. The results of a new test series demonstrated that only the first alteration of the direction leads to an increase of the strain accumulation rate. A comparison of tests with frequently changing amplitudes and tests with the same cycles grouped into packages with constant amplitude confirms that such bundling is conservative, i.e. leads to a slight overestimation of the permanent deformations. Based on another test series it has been demonstrated that monotonic loading paths between bundles of cycles, as they are caused by a change of the average stress, can erase the cyclic preloading history of the sand, i.e. lead to larger cumulative rates in the subsequent bundle of cycles.

Finally, based on axisymmetric triaxial or hollow cylinder triaxial tests, performed on either water-saturated full cylinder samples, dry cuboid-shaped samples with local strain measurements, or water-saturated hollow cylinder samples, the amplitude definition of Niemunis [9] used in the HCA model could be confirmed for 1D to 4D strain paths.

In future, the loss of cyclic preloading history caused by monotonic loading paths will be further investigated. The influence of plastic fines on the sand behaviour under high-cyclic loading has to be clarified as well. The high-cyclic behaviour of partially saturated sands and lightly cemented granular materials will be a matter of future research, too.

Acknowledgements. Parts of the research presented in this paper was performed within the framework of the project "Improvement of an accumulation model for high-cyclic loading" funded by German Research Council (DFG, project Nos. TR218/18-1/2, WI 3180/3-1/2). The authors are grateful to DFG for the financial support. The majority of the cyclic tests have been performed by H. Borowski, P. Gölz and N. Demiral in the IBF soil mechanics laboratory. The tests presented in Section 3 have been conducted by M. Skubisch in the soil mechanics laboratory at RUB.

References

1. Dührkop, J., Grabe, J.: Monopilegründungen von Offshore-Windenergieanlagen - Zum Einfluss einer veränderlichen zyklischen Lastangriffsrichtung. Bautechnik **85**(5), 317–321 (2008)
2. Kaggwa, W.S., Booker, J.R., Carter, J.P.: Residual strains in calcareous sand due to irregular cyclic loading. J. Geotech. Eng. ASCE **117**(2), 201–218 (1991)
3. Ladd, R.S.: Specimen preparation and liquefaction of sands. J. Geotech. Eng. Div. ASCE **100**(GT10), 1180–1184 (1974)
4. Ladd, R.S.: Preparing test specimens using undercompaction. Geotech. Test. J. ASTM **1**(1), 16–23 (1978)
5. Le, V.H.: Zum Verhalten von Sand unter zyklischer Beanspruchung mit Polarisationswechsel im Einfachscherversuch. Dissertation, Fachgebiet Grundbau und Bodenmechanik, Technische Universität Berlin, Issue No. 66 (2015)

6. Miura, S., Toki, S.: A sample preparation method and its effect on static and cyclic deformation-strength properties of sand. Soils Found. **22**(1), 61–77 (1982)
7. Mulilis, J.P., Seed, H.B., Chan, C.K., Mitchell, J.K., Arulanandan, K.: Effects of sample preparation on sand liquefaction. J. Geotech. Eng. Div. ASCE **103**(GT2), 91–108 (1977)
8. Nicholson, P.G., Seed, R.B., Anwar, H.A.: Elimination of membrane compliance in undrained triaxial testing. I. Measurement and evaluation. Can. Geotech. J. **30**(5), 727–738 (1993)
9. Niemunis, A.: Extended hypoplastic models for soils. Habilitation thesis, Publications of the Institute of Soil Mechanics and Foundation Engineering, Ruhr-University Bochum, Issue No. 34, 2003.
10. Niemunis, A., Wichtmann, T., Triantafyllidis, T.: A high-cycle accumulation model for sand. Comput. Geotech. **32**(4), 245–263 (2005)
11. Rudolph, C., Bienen, B., Grabe, J.: Effect of variation of the loading direction on the displacement accumulation of large-diameter piles under cyclic lateral loading in sand. Can. Geotech. J. **51**(10), 1196–1206 (2014)
12. Rudolph, C., Grabe, J.: Untersuchungen zu zyklisch horizontal belasteten Pfählen bei veränderlicher Lastrichtung. Bautechnik **36**(2), 90–95 (2013)
13. Stewart, H.E.: Permanent strains from cyclic variable-amplitude loadings. J. Geotech. Eng. ASCE **112**(6), 646–660 (1986)
14. Sze, H.Y., Yang, J.: Failure modes of sand in undrained cyclic loading: Impact of sample preparation. J. Geotech. Geoenviron. Eng. ASCE **140**(1), 152–169 (2014)
15. Tatsuoka, F., Ochi, K., Fujii, S., Okamoto, M.: Cyclic undrained triaxial and torsional shear strength of sands for different sample preparation methods. Soils Found. **26**(3), 23–41 (1986)
16. Tokimatsu, K.: System compliance correction from pore pressure response in undrained triaxial tests. Soils Found. **30**(2), 14–22 (1990)
17. Towhata, I.: Geotechnical Earthquake Engineering. Springer, Heidelberg (2008)
18. Wichtmann, T.: Explicit accumulation model for non-cohesive soils under cyclic loading. Ph.D. thesis, Publications of the Institute of Soil Mechanics and Foundation Engineering, Ruhr-University Bochum, Issue No. 38 (2005)
19. Wichtmann, T.: Soil behaviour under cyclic loading - experimental observations, constitutive description and applications. Habilitation thesis, Publications of the Institute of Soil Mechanics and Rock Mechanics, Karlsruhe Institute of Technology, Issue No. 181 (2016)
20. Wichtmann, T., Niemunis, A., Triantafyllidis, T.: On the influence of the polarization and the shape of the strain loop on strain accumulation in sand under high-cyclic loading. Soil Dyn. Earthq. Eng. **27**(1), 14–28 (2007)
21. Wichtmann, T., Niemunis, A., Triantafyllidis, T.: Validation and calibration of a high-cycle accumulation model based on cyclic triaxial tests on eight sands. Soils Found. **49**(5), 711–728 (2009)
22. Wichtmann, T., Niemunis, A., Triantafyllidis, T.: Flow rule in a high-cycle accumulation model backed by cyclic test data of 22 sands. Acta Geotechnica **9**(4), 695–709 (2014)
23. Wichtmann, T., Niemunis, A., Triantafyllidis, T.: Improved simplified calibration procedure for a high-cycle accumulation model. Soil Dyn. Earthq. Eng. **70**(3), 118–132 (2015)
24. Wichtmann, T., Triantafyllidis, T.: Strain accumulation due to packages of cycles with varying amplitude and/or average stress - on the bundling of cycles and the loss of the cyclic preloading memory. Soil Dyn. Earthq. Eng. **101**, 250–263 (2017)

25. Wichtmann, T., Triantafyllidis, T.: On the influence of multiple polarization changes on the cumulative deformations in sand under drained high-cyclic loading. Geotech. Test. J. ASTM **43**, 1–18 (2019)
26. Wichtmann, T., Triantafyllidis, T., Späth, L.: On the influence of grain shape on the cumulative deformations in sand under drained high-cyclic loading. Soils Found. **59**, 208–227 (2019)
27. Wichtmann, T., Triantafyllidis, T., Ziesmann, L.: On the influence of platy shell particles on the cumulative deformations in sand under drained high-cyclic loading. Soil Dyn. Earthq. Eng. **117**, 1–15 (2019)
28. Zachert, H.: Zur Gebrauchstauglichkeit von Gründungen für Offshore-Windenergieanlagen. Dissertation, Veröffentlichungen des Institutes für Bodenmechanik und Felsmechanik am Karlsruher Institut für Technologie, Heft Nr. 180 (2015)
29. Zachert, H., Wichtmann, T., Triantafyllidis, T.: Soil structure interaction of foundations for offshore wind turbines. In: 26th International Ocean and Polar Engineering Conference, ISOPE-2016, Rhodos (2016)